Hindawi
International Scholarly Research Notices
Volume 2021, Article ID 2931539, 1 page
https://doi.org/10.1155/2021/2931539

Retraction

Retracted: Properties of PbS: Ni^{2+} Nanocrystals in Thin Films by Chemical Bath Deposition

ISRN Nanotechnology

Received 16 December 2020; Accepted 16 December 2020; Published 26 February 2021

ISRN Nanotechnology has retracted the article titled "Properties of PbS: Ni^{2+} Nanocrystals in Thin Films by Chemical Bath Deposition" [1]. As originally raised on PubPeer [2], significant data duplication was identified with another publication by Lima et al. [3]. The concerns are as follows:

(i) Table 1 shows the same atomic concentrations, and the corresponding EDAX pattern is identical.

(ii) The SEM figures are identical.

(iii) The XRD figures in both articles are identical.

The duplicated data in these publications appear to correspond to the same dataset; however, additional concerns were identified within the article as follows:

(i) Figures 2(b), 2(d), and 2(f) have been duplicated in another publication by the same group, in which a different doping agent, mercury, is used [4]. There is also overlap between Figure 2(b) in [1] and Figure 2(a) in [5], where bismuth is reported as the doping agent.

(ii) Within the article, there is an apparent duplication of Raman spectra in Figure 10 (PbS-Ni6/PbS-Ni4 and PbS-Ni2/PbS-Ni0).

The journal and editorial board are retracting the article due to concerns that the data in this article are not reliable. The authors do not agree to the retraction.

References

[1] O. Portillo Moreno, L. A. Chaltel Lima, M. Chávez Portillo et al., "Properties of PbS: Ni^{2+} Nanocrystals in Thin Films by Chemical Bath Deposition," *ISRN Nanotechnology*, vol. 2012, Article ID 546027, 12 pages, 2012.

[2] *Properties of PbS: Ni^{2+} Nanocrystals in Thin Films by Chemical Bath Deposition*, PubPeer, 2019, https://pubpeer.com/publications/7981935A8A9199C9FB6101338E6150.

[3] H. Lima Lima, C. Aguilar Galicia, A. Camacho Yáñez et al., "Ni influence, on growth of chemically deposited PbS films," *RevistaNaturaleza Y Tecnologia Universidad De Guanajuato*, vol. 2013, pp. 4–11, 2013.

[4] R. Palomino-Merino, O. Portillo-Moreno, L. A. Chaltel-Lima, R. Gutiérrez Pérez, M. de Icaza-Herrera, and V. M. Castaño, "Chemical Bath deposition of PbS: Hg^{2+} nanocrystalline Thin films," *Journal of Nanomaterials*, vol. 2013, Article ID 507647, 6 pages, 2013.

[5] R. Gutierrez Perez, O. P. Moreno, L. Chaltel, and M. Chavez Portillo, "Optical and structural properties of PbS: Bi^{3+} nanocrystals," *Revista Mexicana de Fisica*, vol. 61, pp. 356–362, 2015.

Hindawi
International Scholarly Research Notices
Volume 2021, Article ID 2931539, 1 page
https://doi.org/10.1155/2021/2931539

Retraction

Retracted: Properties of PbS: Ni^{2+} Nanocrystals in Thin Films by Chemical Bath Deposition

ISRN Nanotechnology

Received 16 December 2020; Accepted 16 December 2020; Published 26 February 2021

ISRN nanotechnology has retracted the article titled "Properties of PbS: Ni^{2+} Nanocrystals in Thin Films by Chemical Bath Deposition" [1]. As originally raised on PubPeer [2], significant data duplication was identified with another publication by Lima et al. [3]. The concerns are as follows:

(i) Table 1 shows the same atomic concentrations, and the corresponding EDAX pattern is identical.

(ii) The SEM figures are identical.

(iii) The XRD figures in both articles are identical.

The duplicated data in these publications appear to correspond to the same dataset; however, additional concerns were identified within the article as follows:

(i) Figures 2(b), 2(d), and 2(f) have been duplicated in another publication by the same group, in which a different doping agent, mercury, is used [4]. There is also overlap between Figure 2(b) in [1] and Figure 2(a) in [5], where bismuth is reported as the doping agent.

(ii) Within the article, there is an apparent duplication of Raman spectra in Figure 10 (PbS-Ni6/PbS-Ni4 and PbS-Ni2/PbS-Ni0).

The journal and editorial board are retracting the article due to concerns that the data in this article are not reliable. The authors do not agree to the retraction.

References

[1] O. Portillo Moreno, L. A. Chaltel Lima, M. Chávez Portillo et al., "Properties of PbS: Ni^{2+} Nanocrystals in Thin Films by Chemical Bath Deposition," *ISRN Nanotechnology*, vol. 2012, Article ID 546027, 12 pages, 2012.

[2] *Properties of PbS: Ni^{2+} Nanocrystals in Thin Films by Chemical Bath Deposition*, PubPeer, 2019, https://pubpeer.com/publications/7981935A8A9199C9FB6101338E6150.

[3] H. Lima Lima, C. Aguilar Galicia, A. Camacho Yáñez et al., "Ni influence, on growth of chemically deposited PbS films," *RevistaNaturaleza Y Tecnologia Universidad De Guanajuato*, vol. 2013, pp. 4–11, 2013.

[4] R. Palomino-Merino, O. Portillo-Moreno, L. A. Chaltel-Lima, R. Gutiérrez Pérez, M. de Icaza-Herrera, and V. M. Castaño, "Chemical Bath deposition of PbS: Hg^{2+} nanocrystalline Thin films," *Journal of Nanomaterials*, vol. 2013, Article ID 507647, 6 pages, 2013.

[5] R. Gutierrez Perez, O. P. Moreno, L. Chaltel, and M. Chavez Portillo, "Optical and structural properties of PbS: Bi^{3+} nanocrystals," *Revista Mexicana de Fisica*, vol. 61, pp. 356–362, 2015.

International Scholarly Research Network
ISRN Nanotechnology
Volume 2012, Article ID 546027, 12 pages
doi:10.5402/2012/546027

Research Article

Properties of PbS: Ni^{2+} Nanocrystals in Thin Films by Chemical Bath Deposition

O. Portillo Moreno,[1] L. A. Chaltel Lima,[1] M. Chávez Portillo,[1] S. Rosas Castilla,[1] M. Zamora Tototzintle,[1] G. Abarca Ávila,[1] and R. Gutiérrez Pérez[2]

[1] *Laboratorio de Materials, Facultad de Ciencias Químicas, Benemérita Universidad Autónoma de Puebla, C.U. Puebla, Pue. México, P.O. Box 1067, 72001 Puebla, PUE, Mexico*
[2] *Laboratorio de Síntesis de Complejos, Facultad de Ciencias Químicas, Benemérita Universidad Autónoma de Puebla, P.O. Box 1067, 72001 Puebla, PUE, Mexico*

Correspondence should be addressed to O. Portillo Moreno, osporti@yahoo.com.mx

Received 26 April 2012; Accepted 19 June 2012

Academic Editors: K. G. Beltsios and Y. Song

The growth of nanocrystalline PbS films by chemical bath deposition (CBD) onto glass at temperature $T = 20 \pm 2^{\circ}$C is presented in this research. We report on the modification of structural, optical, and electrical nanostructures due to in situ Ni-doping. The morphological changes of the layers were analyzed using SEM, AFM, and TEM. XRD spectra displayed peaks at 2θ = [26.00, 30.07, 43.10, 51.00, 53.48], indicating growth on the zinc blende face. The grain size determined by X-rays diffraction of the undoped samples was ~36 nm, whereas with the doped sample was 3.2–5 nm. By TEM, the doped PbS was found crystalline films in the range 3.5–5 nm. Optical absorption (OA), and forbidden bandgap energy (E_g) shift disclose a shift in the range 2.1–3.8 eV. Likewise, the dependence of E_g with the radius size and interplanar distance of the lattice is discussed. Raman spectroscopy (RS) exhibited an absorption band ~135 cm^{-1} displaying only a PbS ZB structure. The thermal energy for the films was determined from the slope of dark conductivity (DC) and the energy was estimated to be 0.15 to 0.5 eV.

1. Introduction

The interest into deposition of ternary derivative materials, the potential of designing and tailoring both the lattice parameters and the forbidden bandgap energy (E_g) by controlling growth parameters [1, 2] has grown. In this regard, many techniques have been successfully employed: successive ionic layer and reaction (SILAR) [3], sol gel methods [4], and so forth. Most of the studies reported so far have focused on the deposition of ternary derivatives material in thin films as $Cd_{1-x}Zn_xS$ [5], $Cd_{1-x}SCu_x$ [6], and $Hg_xCd_{1-x}S$ [7]. Noteworthy is the fact that PbS thin films are promising photovoltaic materials as their variable E_g can be adjusted to match the ideal ~1.5 eV required for achieving a most efficient solar cell [8], likewise size-dependent new physical aspects have generated an ongoing thrust for new practical applications, and PbS nanocrystals with grain-size (GS) dimensions in the range 1–20 nm are of technological interest for advanced optoelectronic applications, showing a stronger quantum confinement effect when the crystallite size matches the dimension of Bohr exciton [9]. In this context, there are two situations called the weak confinement and the strong regimes [10]. In the weak regime the particle radius of the electron-hole pair, but the range of motion of the exciton, is limited, which causes a blue shift in the absorption spectrum. When the size of the nanoparticles are below Bohr radius, it leads to the quantum confinement effect. This confinement induces discrete electronic states in the valence and conduction band of the quantum dots compared to the continuous state of energy in bulk material. If the crystallite size is below the exciton Bohr of the semiconductor, strong quantum confinement occurs. The confinement effect appears as a shift in absorption spectra and the absorption to lower wavelengths, which is due to change in the E_g [11, 12] and control over assembly through modification of surface

functionalization. On the other hand, photovoltaic's devices are a widely recognized potential application for nanocrystals due, in part, to their high photoconductivity, easy workup for solutions, and also low cost of production. Several schemes for using nanocrystals in solar cells are under active consideration, including nanocrystals-polymer composites [13, 14]. In this regard, growing interest has been devoted to the Pb-chalcogenide family for nanocrystals solar cell applications because they have such large exciton Bohr radii of 18 nm, in the limit where the nanocrystals are only a tenth part or so of the bulk exciton diameter: electrons and holes can then tunnel through a thin surface coating, and therefore strong electronic coupling between particles allows the transport of charge between nanocrystals. The quantized electronic transitions in Pb(S, Se) nanocrystals quantum dots (NQDs) have been reported to provide size-tunable interband absorption and luminescence emission at a broad and technically important infrared wavelength range, spanning from 0.8–4.0 μm [15]. It must be pointed out that the synthesis of ternary $Pb_{1-x}Ni_xS$ nanocrystals remains largely underdeveloped compared to the widely studied cadmium chalcogenide. Thus, on this frame of reference, in the present work attempt has been made to prepare PbS and Ni^{2+}-doped PbS nanostructured films by CBD, in order to investigate structural, optical, and electrical properties of undoped and doped-PbS films. Surface morphology and composition were determined using a Carl Zeiss Auriga 39-16 coupled with a Bruker energy dispersive analysis of X-Rays (EDAX). The crystalline structure characterization was carried out by XRD patterns registered in a D8 discover diffractometer, using the Cu K_α line. The grain size was determined utilizing the Scherer´s formula on XRD patterns. The optical absorption spectra, measured by employing a Unicam 8700 Spectrometer, allow calculation of the forbidden bandgap energy (E_g) by using the $(\alpha h\nu)^2$ versus $h\nu$ plot, where α is the optical absorption coefficient and $h\nu$ is the photon energy. Transmission electron microscopy was performed using a Philips CM 300. The Raman spectra were determined with a micro-Raman System Lab Ram-Idler apparatus with an excitement line of 632.8 nm. Dark conductivity measurements as a function of absolute temperature over the temperature range of 100–500 K were achieved by using a closed cavity coupled to a vacuum system with a pressure of 10^{-2} mbar. A Keithley 617 programmable electrometer with accuracy of $\Delta l = \pm 0.005$ pA, $\Delta V = \pm 0.0025$ V, and a DL4600 deep level transient spectrometer with an accuracy of $\Delta T = \pm 0.05$ K were employed for sheet resistivity measurements.

2. Chemical Reactions and Experimental Procedure

The reactions for the growth of PbS films doped with Ni^{2+} were determined by employing the cell potential values in basic media reported [16]. The cell potential and the Gibbs free energy are related through the Nernst equations: $\Delta G^o = -n\tau\varepsilon^o$, where n is the number of equivalents, τ is the Faraday constants, ε^o are the cell potential, and ΔG^o is calculated for the reaction. Value ΔG^o provides thermodynamic information on the spontaneity of chemical reactions. Worth noting is the formation of the coordination complex $[M(NH_3)_4]^{2+}$, which is determinant for the release of M^{2+} ions ($M^{2+} = Cd^{2+}$, Pb^{2+}, Zn^{2+}, etc.) and their slow recombination with S^{2-} ions that, under these conditions, leads to the spontaneous formations to the MS precipitate in an easily controlled process. The growth of PbS is therefore carried out according to the following steps: (a) by mixing $Pb(CH_3CO_3)_2$, KOH, and NH_4NO_3, the coordination complex $[Pb(NH_3)_4]^2$ is generated indirectly. (b) The S^{2-} ions are found in the solution and are generated by the thiourea decomposition in alkaline solution. (c) The aforementioned steps allow the slow process at the substrate surface to take place predominantly over direct hydrolysis of thiourea in the bulk of the reaction bath as follow [17]:

$$SC(NH_2)_2 + 3OH^- \Longleftrightarrow CH_2N_2 + CO_3^{2-} + H_2S + 3H^+ \quad (1)$$

$$HPbO_2^- + H_2O + 2e \Longleftrightarrow Pb + 3OH^- \qquad \Delta G^0 = +104.2\,\text{KJ}. \quad (2)$$

Leading to complex (II)

$$[Pb(NH_3)_4]^{2+} + 2e \Longleftrightarrow Pb + 4NH_3 \qquad \Delta G^0 = +180.3\,\text{KJ}, \quad (3)$$

$$Pb^{2+} + 2e \Longleftrightarrow Pb \qquad \Delta G^0 = +24.31\,\text{KJ}. \quad (4)$$

Changing the sense of (4) and added with (3)

$$[Pb(NH_3)_4]^{2+} \Longleftrightarrow Pb^{2+} + 4NH_3 \qquad \Delta G^0 = +155.99\,\text{KJ}. \quad (5)$$

The reaction of PbS for the formation of the S^{2-} ion and elemental Pb is, therefore:

$$Pb + S^{2-} \Longleftrightarrow PbS + 2e \qquad \Delta G^0 = +179.49\,\text{KJ}. \quad (6)$$

Addend (5) and (6)

$$[Pb(NH_3)_4]^{2+} + Pb + S^{2-} \Longleftrightarrow PbS + Pb^{2+} + 4NH_3 \qquad \Delta G^0 = +335.48\,\text{KJ}, \quad (7)$$

$$S + 2e + 2H^+ \Longleftrightarrow H_2S \qquad \Delta G^0 = -27.40\,\text{KJ}. \quad (8)$$

Addend (7) and (8).

Changing the sense of (8) and added with (7)

$$[Pb(NH_3)_4]^{2+} + H_2S + S^{2-} \Longleftrightarrow PbS + 4NH_3 + S + 2H^+ + 2e \qquad \Delta G^0 = +362.88\,\text{KJ}, \quad (9)$$

$$HPbO^- + H_2O + 2e \Longleftrightarrow Pb + OH^- \qquad \Delta G^0 = +436.61\,\text{KJ}. \quad (10)$$

Addend (9) and (10)

$$HPbO^- + H_2O + [Pb(NH_3)_4]^{2+} + H_2S + S^{2-} \Longleftrightarrow PbS + 4NH_3 + S + 2H^+ + Pb + OH^- + Pb^{2+} \qquad \Delta G^0 = +799.48\,\text{KJ}. \quad (11)$$

Since $\Delta G^0 > 0$, and as such, the reaction is not a spontaneous process.

Reversing the direction of the reaction (6), ΔG^0 changes its sign:

$$\mathrm{PbS} \Longleftrightarrow 2e + \mathrm{Pb} + \mathrm{S}^{2-} \qquad \Delta G^0 = -179.4\,\mathrm{KJ}. \tag{12}$$

For sulfur ion

$$\mathrm{S}^{2-} \Longleftrightarrow \mathrm{S} + 2\mathrm{e} \qquad \Delta G^0 = +86.272\,\mathrm{KJ}. \tag{13}$$

Adding (4), (5), and (6), the reaction for the PbS is obtained

$$\mathrm{Pb} + 2\mathrm{S}^{2-} + \mathrm{H}^+ \Longleftrightarrow \mathrm{PbS} + \mathrm{HS}^- \qquad \Delta G^0 = -120.50\,\mathrm{KJ}, \tag{14}$$

$$\mathrm{PbS} + 2\mathrm{e} + 2\mathrm{H}^+ \Longleftrightarrow \mathrm{Pb} + \mathrm{H_2S} \qquad \Delta G^0 = +177.66\,\mathrm{KJ}, \tag{15}$$

$$\mathrm{Ni}^{2+} + 2\mathrm{e} \Longleftrightarrow \mathrm{Ni} \qquad \Delta G^0 = +48.250\,\mathrm{KJ}, \tag{16}$$

$$\mathrm{Ni} + 2\mathrm{OH}^- \Longleftrightarrow \mathrm{Ni(OH)_2} + 2\mathrm{e} \qquad \Delta G^0 = -138.96\,\mathrm{KJ}, \tag{17}$$

$$\mathrm{Ni(OH)_2} \Longleftrightarrow \mathrm{Ni}^{2+} + \mathrm{OH}^- \qquad \Delta G^0 = 90.71\,\mathrm{KJ}. \tag{18}$$

Adding (14) and (18), the reaction for the PbS : Ni2+ entity is obtained:

$$\mathrm{Pb} + 2\mathrm{S}^{2-} + \mathrm{Ni(OH)_2} \Longleftrightarrow \mathrm{PbS} + \mathrm{HS}^- + \mathrm{Ni}^{2+} + \mathrm{OH}^- \qquad \Delta G^0 = -29.79\,\mathrm{KJ} \tag{19}$$

Based on the Gibbs free energy values obtained from the thermodynamic equilibrium analysis, the Ni^{2+} ionization state probably is present in the volume of PbS under our work conditions comparing the changes in ΔG^0, which thermodynamically enable the growth of the PbS : Ni^{2+}. Deposition includes different limiting physical and chemical processes which determine the kinetic behaviour of the doped PbS. (i) Nucleation stage. It is the initial stage requiring a high activation energy in which reactive centres (nuclei) are formed on the surface on the substrate. (ii) Growth stage. It is the second stage, which is characterized by an enhanced rate of PbS deposition. (iii) Doped stage. The high rate of deposition is associated with the addition level of doping, with the accelerated growth of PbS doped nuclei formed on the substrate during the nucleation stage. (iv) Termination stage. During this stage, the rate of deposition gradually slows down. This is probably due to a depletion of the reagents in deposition mixture. Preparation of polycrystalline PbS thin films on glass substrates was performed at a temperature of 20 ± 2°C undoped and doped with $V_{[Ni^{2+}]}$ grown by chemical bath deposition (CBD) and pH = 11.0. The glass substrates were previously immersed in a $K_2Cr_2O_7$/HCl/H_2O solution for 24 h, after which they were rinsed in deionised water and dried in a clean hot air flow. The growth of PbS films with six different levels of doping $V_{[Ni^{2+}]}$ was obtained by the addition in situ: 2, 4, 6, 8, 10, 12 mLs in the solutions for PbS growth $Pb(CH_3CO_3)_2$ (0.01 M), KOH (0.5 M), NH_4NO_3 (1.5 M), $SC(NH_2)_2$ (0.2 M). The solutions were mixed and the final solution heated at 20 ± 2°C during 2 h, with the substrate remaining inside the solution. The optimal concentration of the doping solution $[V_{[Ni^{2+}]}]$ $Ni(NO_3)_2$ (0.023 M) was determined after several trials, until films had attained good adherence. This solution is routinely added to the reaction mixture during the growth of the PbS films. All the used solutions were prepared with deionised water of resistivity 18.2 MΩ. The samples were labelled as PbSNi0 for the undoped sample and PbSNi2-PbSNi12 for the doped samples. The total volume of the growing-solution consisted of the volume-solution (V_{PbS}) for the PbS growth plus the volume-solution $V_{[Ni^{2+}]}$ containing the doping Ni^{2+} chemical agent: $V_{PbS} + V_{[Ni^{2+}]} = V_{tot}$. The relative volume $V_{[Ni^{2+}]}$ changed from 2 to 12. The obtained growing films were silver-colored, polycrystalline-reflective, with a homogeneous consistency and good adhesion to the substrate.

Table 1: Atomic concentrations of Pb, S and Ni obtained from SEM.

	Atomic concentrations		
Sample	Pb	S	Ni
PbS-Ni0	56.35	43.05	0.0
PbS-Ni6	70.10	18.38	11.51
PbS-Ni12	56.29	33.49	10.22

3. Results and Discussion

Figure 1 displays a typical EDAX pattern and details of a relative analysis for (a) undoped (b) doped-PbS. The elemental analysis was performed only for Pb, S, and Ni, deriving the average atomic percentage of undoped and doped Pb/S. The semiquantitative analysis of the films was carried out by using the EDAX technique for undoped and doped PbS thin films at different points to study the stoichiometry of the films. In Table 1 are displayed the atomic concentrations of Pb, S, and Ni. For the samples, the increase in concentration of Ni in PbS films is easily noted, reaching a percent value of Ni = 11.51. In this case, when Ni^{2+} ion enters as a substitute for the Pb^{2+} ion, it is observed that the sample was slightly deficient in S^{2-} ion. Therefore, for the higher $V_{[Ni^{2+}]}$ values considered here, growth material can probably be estimated as doped semiconductor but actually the material can be regarded as similar to a solid solution of $Pb_{1-x}Ni_xS$. It can also be considered how the concentration of Ni in PbS films increases, reaching a percent value of Ni = 11.51. In this case, when the Ni^{2+} ion enters as substitute for the Pb^{2+} ion, probably for the higher $V_{[Ni^{2+}]}$ values considered here, the growth material can also be estimated as a doped semiconductor being the material also as in the aforementioned conditions similar to a solid solution of $Pb_{1-x}Ni_xS$. The micrographs of undoped and doped PbS films are showed in Figure 2. Scale bar at 1.0 μm and 30 nm, respectively, were obtained from scanning electron spectroscopy (SEM). The undoped-PbS0Ni, doped-PbSNi6, doped-PbS12Ni films are showed. As can be seen from the

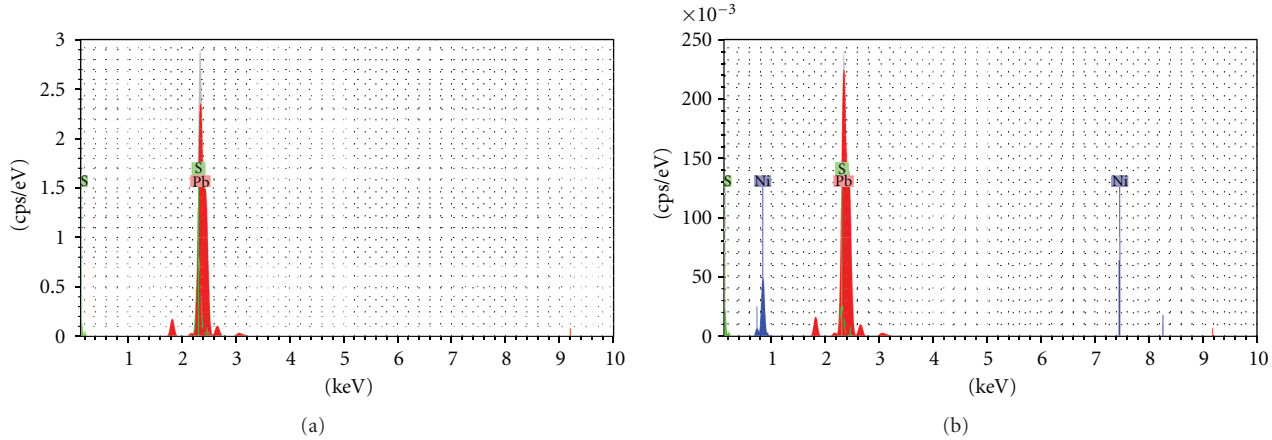

Figure 1: EDAX patterns (a) undoped-PbS0Ni, (b) doped-PbS12Ni, with 12 mLs.

uniform surface morphology, such aspect is compact and of polycrystalline nature. The SEM micrographs show that the particle grain size decreases with an increase in $V_{[Ni^{2+}]}$ concentration. The granules appeared to be of different sizes and it can be concluded that the doping plays a vital role in the morphological properties of the thin PbS films. The micrographs of the films with doping levels of $V_{[Ni^{2+}]}$ 2, 4, 8, and 10 mLs are not shown. In such micrographs for the undoped films, crystals as small spheres are observed. A very adherent film with metallic gray-black colour aspect was obtained for undoped and doped films revealing continuous and compact polycrystalline films. Similar morphologies have been reported by Pentia et al. as an effect of the reducer Bi^{3+} ion on the deposition by CBD [18].

The undoped and doped PbS thin films were characterized using atomic force microscope (AFM) technique. Figure 3 shows the undoped and doped PbS samples. In this Figure, the tree-dimensional representation of PbS is showed: (a) undoped PbSNi0, (b) doped PbSNi6, and (c) doped PbSNi12. The images for films with doping levels of 2, 4, 8, and 10 mLs are not shown. In Figure 3(a) The PbSNi0 indicates that the growth of small and irregular grains distributed is rather different from each other, indicating irregular growth rate of the grains. (b) With respect to PbSNi6 sample, the reduced grain density indicates the smaller grain of doped-PbS $V_{[Ni^{2+}]}$. The surface roughness is unavoidable since the grains are grown in different sizes. Figure 3(c) PbSNi12 shows that the small spherical nanograins of approximately 4-5 nm size were uniformly distributed over the smooth homogeneous background crystalline phase. Since the Gibbs free energy of the surface of small-size nanoparticles is usually very high due to large surface-to volume ratio, these small particles have tendency to aggregate together to decrease the Gibbs free energy of surface and make the surface state stable.

Figure 4 shows diffractograms of X-ray (XRD) for doped and undoped films. Such X-ray spectra display peaks located at the following angular positions: $2\theta = [26.00, 30.07, 43.10, 51.00, 53.48]$. They are related with the reflection peaks of (111), (200), (220), (311), (222), respectively, and all these diffraction peaks can be perfectly indexed to diffractograms of the undoped and doped PbS samples displaying the zinc blende (ZB) crystalline phase according to reference patterns JCPDS 05-0592. The XRD spectra for PbSNi2 films indicate that (111) is the orientation of PbS Ni grains; the PbSNi2 diffraction layer along with the (111) plane reveals the highest intensity of a well-defined sharp peak, indicating the high crystallinity of the obtained material. A maximum value in the intensity peak is reached for the prepared sample, indicating either the existence of a larger number of (111) planes or that the (111) planes have a lower number defects. The relative intensities for PbSNi2 and PbSNi4 layers for (111), (200), (220) are nearly equal and all the representative diffraction lines of PbS can be observed. In the PbSNi2 film, the (111) reflection has the highest intensity. This phenomenon may be attributed to the doping effect. The low intensity peaks observed in the XRD patterns of the doped PbSNi6 to PbSNi12 samples indicate that the films are coarsely fine crystallites or nanocrystalline. The broad hump in the displayed pattern is due to an amorphous glass substrate and also possibly due to some amorphous phase present in the PbSNi crystallite size of films. There are two main possible causes for peak broadening. The first is increase in heterogeneity of the films due to the occupation of Ni^{2+}into the host lattice. A second cause is a decrease in crystallite size. These effects are associated with the nanocrystals doped-PbSNi with $V_{[Ni^{2+}]}$ in the regime were the cluster mechanism is dominating (on the contrary to films grown via ion-ion mechanism, were the crystal size was larger) and consists of PbSNi nanocrystals embedded in an apparent matrix of PbS. The inset in Figure 4 displays the (111) interplanar distance (ID) for the ZB face, calculated from the 2θ peak positions, versus $V_{[Ni^{2+}]}$. This ID is close to the (111) ID of the ZB phase. First, the ID decreased with $V_{[Ni^{2+}]}$ due to the presence of Ni^{2+} in substitution sites and, finally, reaching a maximum value in PbSNi6 film. A possible explanation to this experimental fact can be given as follows: The ionic radii data are Pb^{+2} = 1.21 Å, S^{2-} = 1.84 Å, and NI^{2+} = 0.69 Å, therefore, for a relative low concentration of Ni^{2+} ions a majority can be located in (i) Pb^{2+} vacancies sites, which otherwise would be empty, (ii) in Pb^{2+} sites causing the appearance of Pb interstitial, and

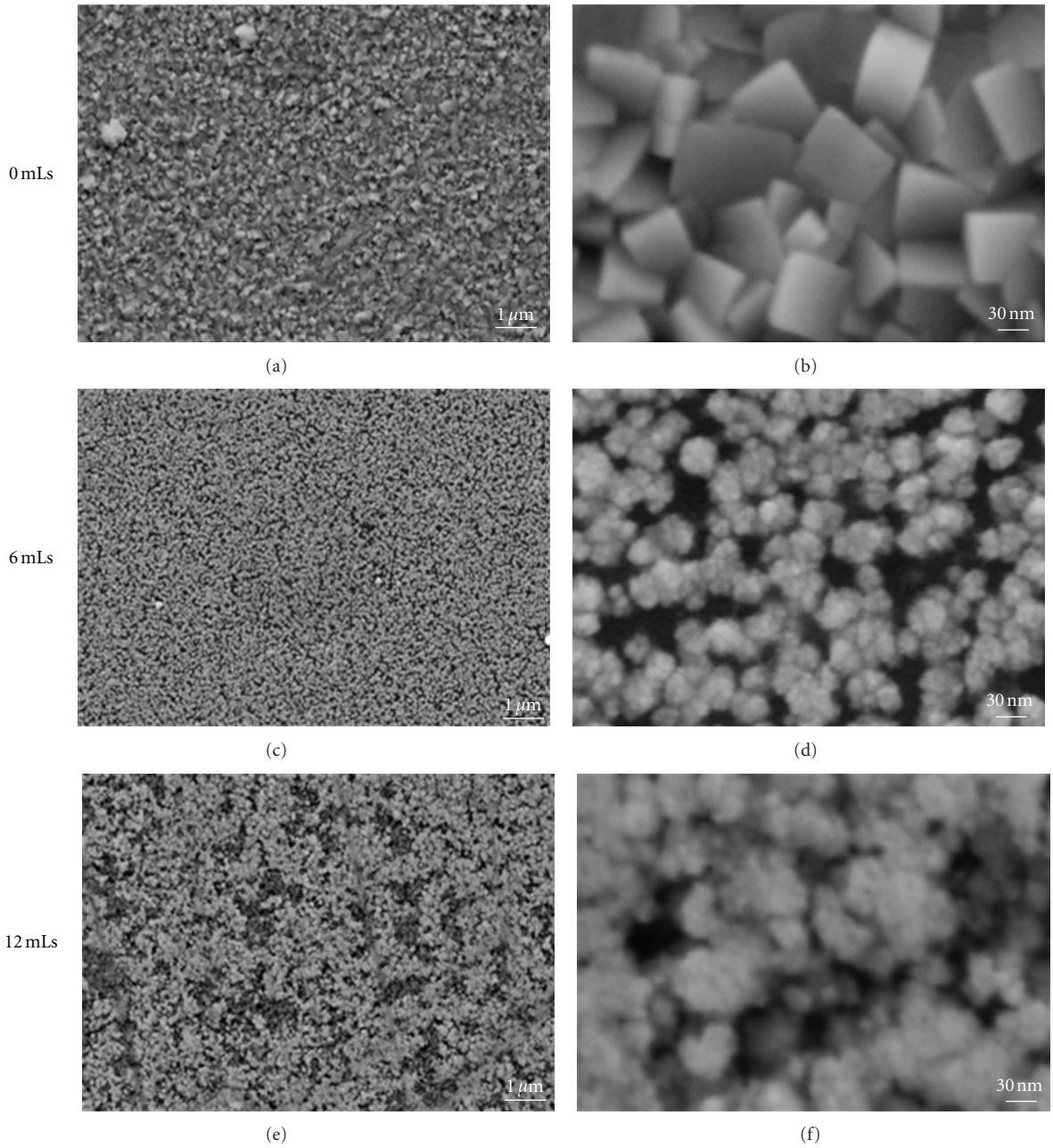

Figure 2: Micrographs of the films with scales of 1.0 μm and 30 nm for undoped-PbSNi0, PbSNi6, and PbSNi12-films.

(iii) in interstitial positions. It can be mentioned that the stable crystal structure of PbS, as a result, when Ni^{2+} occupies more and more sites of Pb^{2+} in the host lattice, internal strain would arise, and the crystal structure of PbSNi solid solution becomes unstable. In order to stabilize the crystal structure, the grain size is reduced to release the strain. As the Ni^{2+} concentration is increased, the diffraction peaks become broader due to reduction in the grain size. At this level of $V_{[Ni^{2+}]}$, the PbSNi can be considered a doped material [6]. The incorporation of Ni^{2+} solubility has been proven to be more effective in Pb chalcogenide than Zn-chalcogenide, a result explained in terms of the cation size.

The crystal structure of the PbS undoped and doped films has been studied by transmission elestron microscopy (TEM). A typical bright plan view obtained by TEM image of the nanoparticle PbS films is shown in Figure 5, TEM images of nanocrystals and their respective selected area electron diffraction (SAED) pattern of plain core (PbS): (a) Undoped-PbSNi0 (b) Doped-PbSNi6 (c) y (d) An HRTEM of PbSNi12 and core-shell nanocrystals, shows a clear (111) an (200) lattice fringe with crystal plane spacing 0.34 nm 0.96 nm, respectively. The inset illustrates selected-area electron diffraction (SAED) pattern of plain core (PbS) and core-shell nanocrystals is displayed. Such

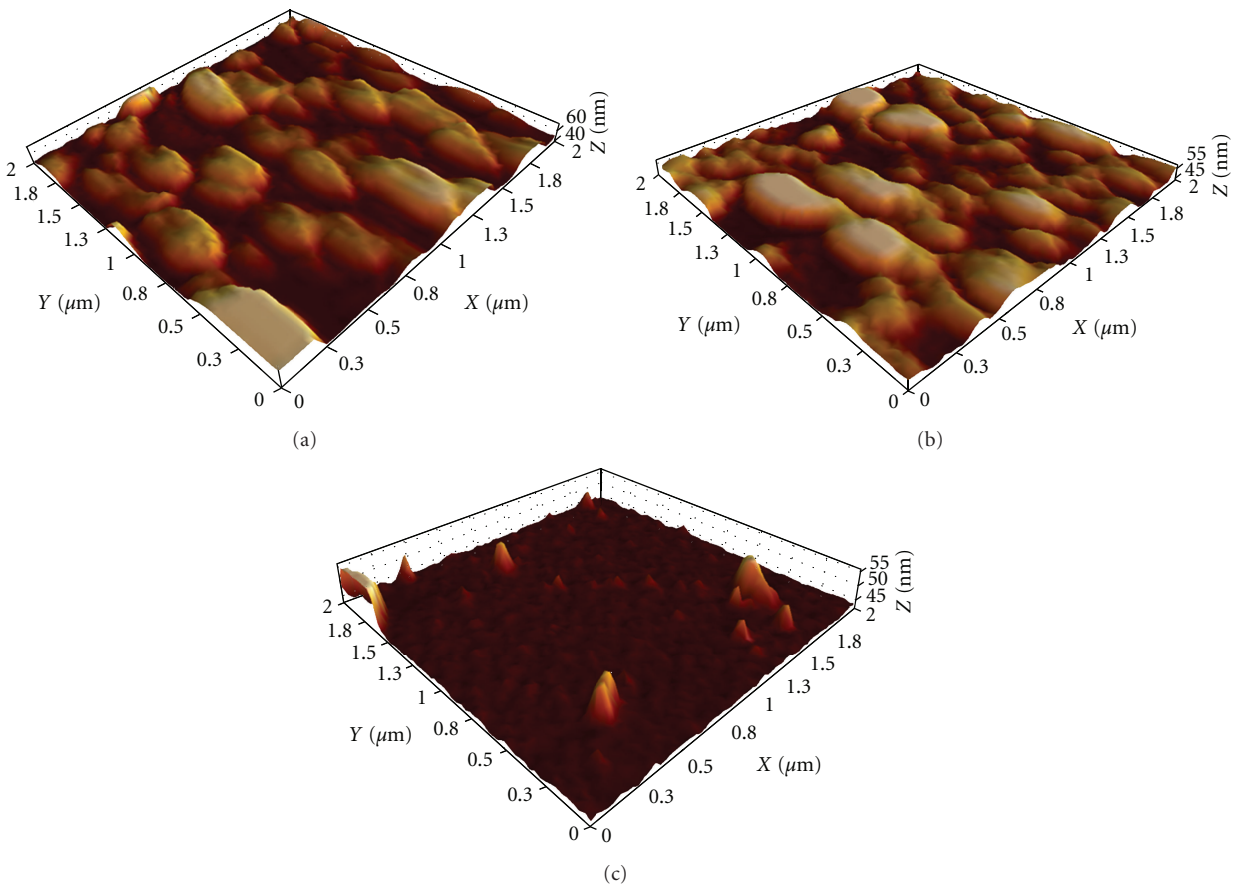

Figure 3: Three-dimensional representation of PbS films using AFM. (a) Undoped-PbSNi0. (b) Doped-PbSNi6. (c) Doped-PbSNi12.

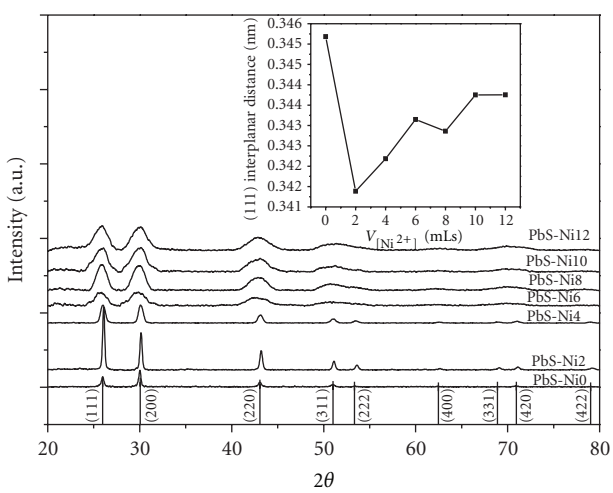

Figure 4: XRD diffractograms for doped and undoped-PbS films. The patterns are placed consecutively. The inset illustrates the (111) reflections of the cubic phase as function of $V_{[Ni^{2+}]}$.

results revealed that small particles attach together with a common crystallographic orientation, and most of the produced crystals have irregular shapes. The sizes of the clusters are mostly 3.5–5 nm. The micrographs with an electron beam direction close to (111) zone axis in strongly under focused condition and as such, the black/gray contrast in white background represents the PbS nanoparticle in the range 3.5–5 nm. The average grain size (GS) in the films is observed to decrease while doping is increasing. Samples are found to be crystalline by TEM, a feature which is very similar to size calculated from XRD peak width. The ZB phase is detected for all the nanoparticle films from XRD data. The sharp rings presented in SAED patterns are indicative of polycrystalline nature of the films. The SAED patterns were analyzed using the standard procedure. The SAED pattern with clear spots indicates perfect orientation around (111) pane. The blurring of the diffraction ring in the selected-area electron diffraction (SAED) pattern of core-shell nanocrystals in comparison to that of plain core structures revealed the deposited nanoparticle thin films. From this measurement, it is clear that both undoped and doped films are polycrystalline in nature.

Figure 6 shows a graph of E_g versus $V_{[Ni^{2+}]}$ and in the inferior right part the plot shows the absorption spectrum for the sample PbSNi12. In this plot, it can be observed an E_g = 2.4 eV value for the PbSNi0 sample. For PbSCd0 sample, through the intersection of the straight line with the axis of the photon energy, an E_g value is obtained in a similar way to all samples. The confinement effect appears as a shift in edge of the absorption spectra and the

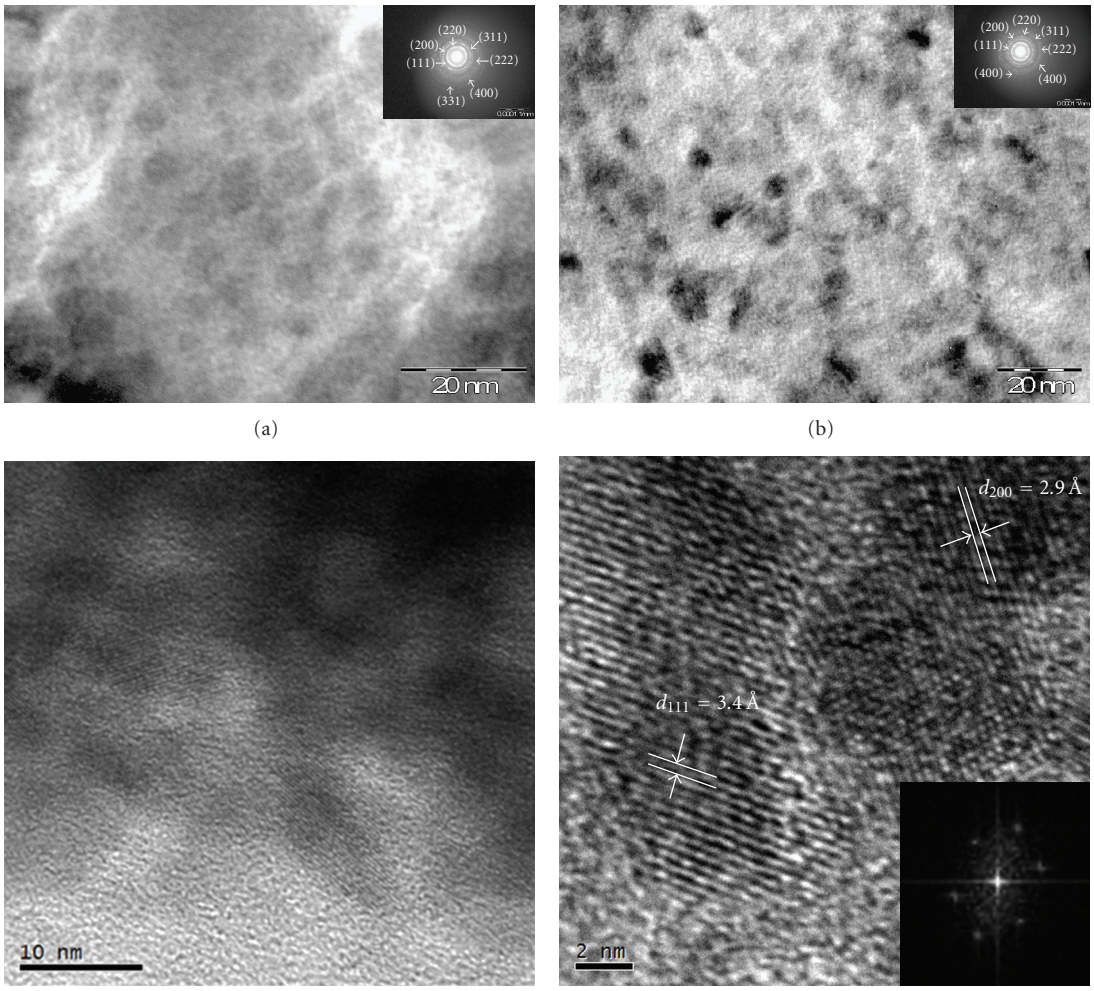

Figure 5: TEM images of nanocrystals: (a) undoped-PbSNi0 (b) doped-PbSNi6 (with 6 mLs). (c) y (d) an HRTEM of PbSNi12 and their respective selected area electron diffraction (SAED) pattern of plain core (PbS) and core-shell nanocrystals.

absorption to lower wavelengths, possibly due to the decrease in GS, the decrease in number of defects and the change in color. It is clearly seen from the optical spectrum an absorption edge shift toward a lower wavelength in doped films. This clearly indicates a considerable increase in the bandgap as a result of Ni-doping. Doping of PbS with Ni is expected to alter the optical bandgap between 0.41 eV (E_g of PbS) and the resulting ternary PbSNi alloy. Thus, the observed large modification of ternary PbSNi alloy and the existence of strong quantum confinement in this system. The experimentally observed E_g values for the shift indicated an alloying between nanocrystalline PbS. Such increase has been observed by other authors [19, 20]. The E_g for doped samples in the 2.4–3.8 eV range the large experimentally observed E_g in the nanoparticle films theoretically estimated (using Vegar′ds law) E_g for bulk shows the extent of quantum size effect in the nanoparticle films. The fundamental optical transition of doped films (E_g = 0.41 eV) is not observed in these films, presumably because of complete mixing of PbS with Ni^{2+} affording a unique ternary intermetallic compound of the $Pb_xNi_{1-x}S$ type [1]. It is observed that the size effect on the optical bandgap is stronger in nanoparticle films than in PbS nanoparticle of 24–10 nm (average crystallite size) and shows an E_g: 2.22–2.65 eV [2]. The observed increase in the quantum size effect could possibly be attributed to a decrease in the effective mass [21]. The increased in E_g when increasing the concentration of $V_{[Ni^{2+}]}$ in the films is reflected by the presence of an excitonic structure material. Excitonic structures are readily observed in large E_g semiconductors with binding energy such as CdSe [22]. The E_g optical doped films varied from 2.4 to 3.8 eV, with doping increase of $V_{[Ni^{2+}]}$. A similar shift observed in the position of the excitonic peak towards higher energies in CdSe crystallites has been explained due to a decrease in crystallite size [23]. The redshift of the bandgap is associated with the decline of the SG. It is clear that the E_g increases when $V_{[Ni^{2+}]}$ increases. As mentioned earlier, we observed a systematic decrease in the crystallite size with increasing concentration. Since the estimated mean crystallite size in this case is approximately half the value of the exciton Bohr radius in

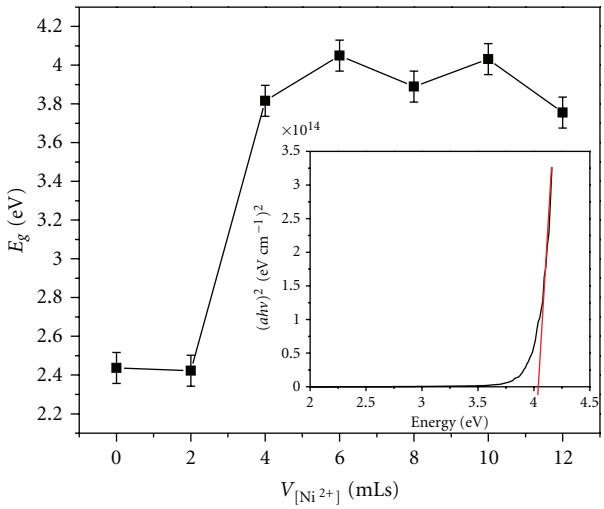

Figure 6: The bandgap energy (E_g) as function of $V_{[Ni^{2+}]}$. The inset illustrates the method to calculate E_g from optical absorption measurements.

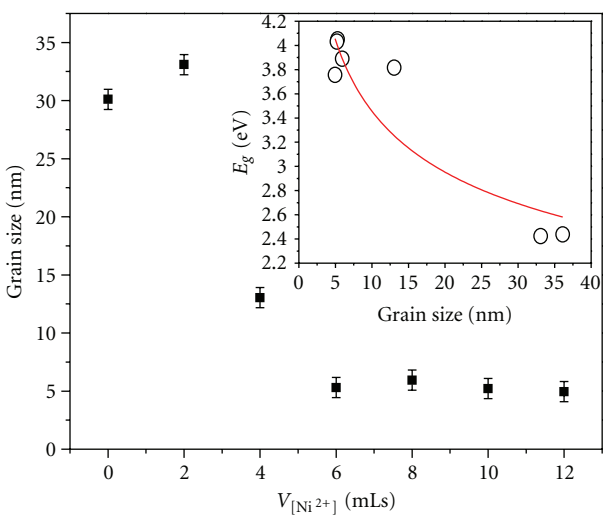

Figure 7: The average grain size (GS) with of the mean peak of XRD patterns versus $V_{[Ni^{2+}]}$. The inset exhibits the E_g versus GS plot.

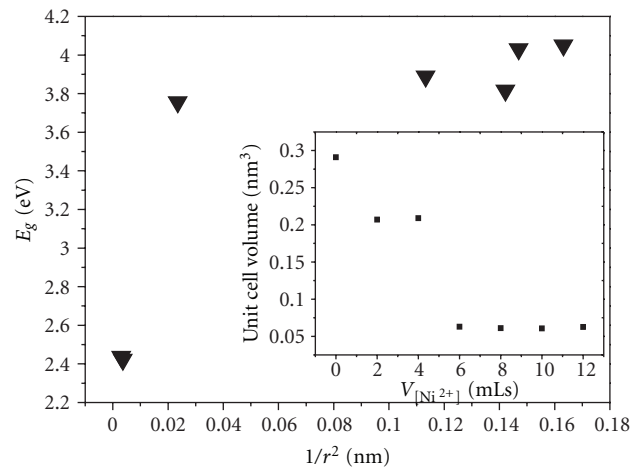

Figure 8: E_g data plotted against the inverse square of the average radius of grain $1/r^2$ The inset displays the unit cell volume as function of V (mLs) $V_{[Ni^{2+}]}$.

PbS, we observe a strong confinement in doped PbSNi films. Using already published data, a nanocrystalline size of 4-5 nm corresponding to E_g = 1–1.25 eV, 3.8 nm for E_g = 1.4 eV, 2.7 nm for E_g = 2.0 eV, and 2 nm for E_g = 2.7-3.8 eV, respectively are obtained [24].

Figure 7 shows the average grain size (GS) versus $V_{[Ni^{2+}]}$ for the undoped- and doped PbS samples corresponding to the (111) plane. In this figure, it can be observed that GS reduces in the interval 4 mLs $\leq$ $V_{[Ni^{2+}]}$ $\leq$ 12 mLs. It can be seen for the PbSNi0, GS ~32 nm, that the GS decreases for doped samples. The effect of the GS decrease by the doping effect has been reported in films of CdS doped with Cu^{2+} by CBD [6]. A decrease in the degree of order of crystallites is expected to lead to enhanced growth of stable nuclei at the initial stages of growth, followed by impaired grain growth, and hence resulting in smaller grains in the nickel. In the inset of Figure 6, E_g is displayed as function of the GS. For low GS, E_g increases, as GS decreases E_g increase. When GS $\cong$ 5 nm, E_g reaches a maximum value. For a larger GS, E_g decreases. Two effects can be considered in such E_g changes: (i) the variation of ID and (ii) the strong quantum confinement.

In Figure 8, the E_g versus $1/r^2$ has been plotted, where r is the average radius (r = GS/2) by considering, as a good approximation, the grain spheres of PbS for the undoped and doped samples. The well-known linear dependence of E_g as function of $1/r^2$ resembles each other. This E_g versus $1/r^2$ plot would correspond to a strong confinement regime, as the Bohr radius is 18 nm and the smallest average radius found in PbSNi6 films is 5 nm. As can be seen, E_g data plotted as the inverse square of the average radius of grain $1/r^2$ ID increases and GS decreases. Such ID effects on E_g display, however, the ID effects predominate as E_g diminishes; for r > 5 nm, ID decreases, and as a result the combined effects are to increase the E_g value. The inset in Figure 8 displays the unit cell volume (UCV) versus $V_{[Ni^{2+}]}$ function. As expected, UCV has a similar dependence with IDs versus $V_{[Ni^{2+}]}$; this type of plot has been reported when Cu^{2+} in CdS is either decreasing or increasing [6]. To the best of our knowledge, no dependence between IDs and GS has been found in theoretical approaches and experimental findings on doped and undoped nanocrystals reported [6, 21, 22]. Figure 9 exhibits the (111) interplanar distance (ID) as function of the average GS, and in inset the 1/GS versus unit cell volume (UCV) is displayed. The 1/GS represents the inverse of average diameter of nanoparticles. This figure resembles a close and direct proportionality between UCV and 1/GS. A linear dependence between these two parameters can be observed. As expected, UCV has a similar dependence with ID versus $V_{[Ni^{2+}]}$. In general, a decreasing of both ID when GS increases can be observed with, roughly, a linear inverse dependence, independent if $V_{[Ni^{2+}]}$ is either

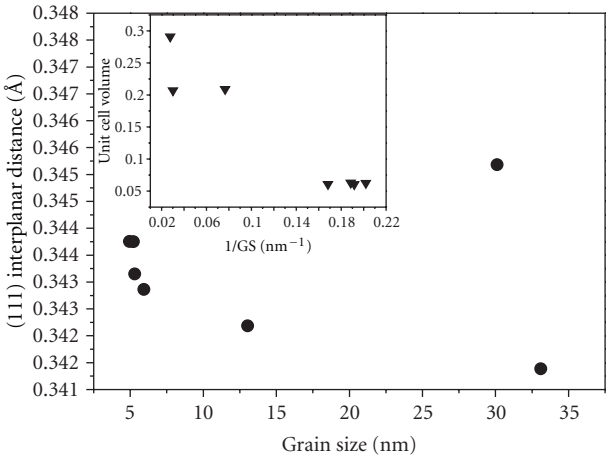

Figure 9: (111) interplanar distance (ID) as function of the average grain size (GS). The inset shows the unit cell volume versus $V_{[Ni^{2+}]}$.

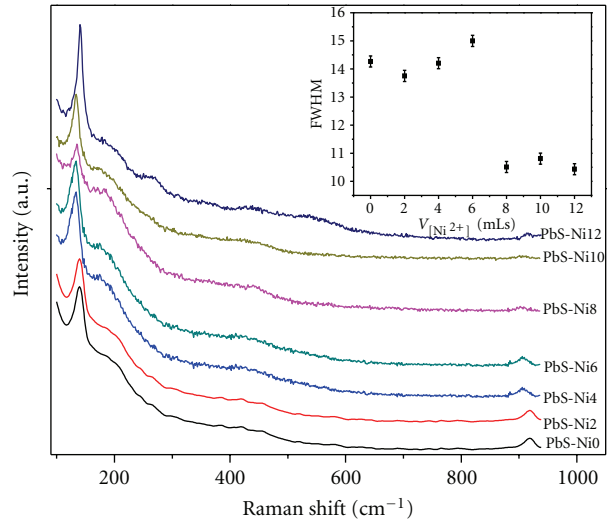

Figure 10: Raman spectra for the undoped and doped-PbS films. The inset exhibits the FWHA.

decreasing or increasing. As above, no dependence between ID and GS has been found in theoretical approaches and experimental findings on doped and undoped nanocrystals reported in the literature, except a couple of experimental works [25, 26] with no further explanation. The strong strains introduced by the foreign ions promote changes in the interatomic distances and hence in the ID. The UCV versus 1/GS plot—where 1/GS represents the inverse diameter of the nanoparticles is displayed in the inset of Figure 9, suggesting that the strong strains introduced by others atoms relax at the surface of the grains. The effect of this relaxing in the inner of the particle must be more evident for smaller grains and ID will become larger. If, inversely, there exists a growing relaxing on the lattice, the increase of ID will be easier for smaller particles. In this way, UCV and GS have an inverse dependence. In our case, the introduction of Ni^{2+} ions into PbS promoted the rise of strains. On the other hand, the creations of S^{2-} vacancies relax the lattice. Strains, in PbSNi, tend to reduce GS with an ID increased. Likewise, relaxing tends to reduce GS, with an ID increased. Relaxing tends to recover the initial values of GS and ID. When doping, the number of the nucleation centers increases both on the substrates and the solution and, in this way, the nucleation rate becomes larger than the growth rate leading to a broader dispersion in GS and to a decrease of this one.

The 514.5 nm wavelength laser Raman spectroscopy was used to analyze the films. The spectra displayed doped and doped PbS films in Figure 10 show that the same wavenumbers at 135, 217, 433, and 647 cm^{-1} peaks corresponded to the fundamental longitudinal optical (LO) phonon mode of rock-salt structure, first overtone (2LO) and second overtone (3LO), respectively. The inset of Figure 10 displays the $V_{[Ni^{2+}]}$ versus the width at half maximum (FWHM). The behaviour of the FMHA values of the SR confirms that the crystalline quality of the material is better for high doped level, in according with the TEM and XRX measurements, respectively. The strong band in ~133–140 cm^{-1} is attributed to a combination of longitudinal and transversal acoustic modes. However the position and intensities of Raman peaks were also influenced by difference in particles sizes [27]. It has been reported that the band centred at 961 cm^{-1} could be due to sulphates in the sample not the laser-induced degradation [28], which is consistent with reported results [29]. However, in our samples, the XRD patterns of PbS undoped and doped structures confirms that the product consists of PbS pure cubic without the presence of sulphates. It should be noted that data from PbS nanoparticles (18 nm in diameter) in a room air temperature have shown that the LO band to be at ~210 cm^{-1} with a small shoulder, attributed to an SP mode, at 205 cm^{-1}, however, a downward trend in wave number was shown for the former as the size of particles was increased to 35 nm diameter [30].

Figure 11 shows the plot of logσ as a function of T^{-1} in the temperature of 100–500 K range for the undoped- and doped-PbS films. The dark activation energy E_a was determined for samples from the slope of the high-temperature range of the corresponding curves in accordance with the relation $\sigma = \sigma_0 \exp(-E_a/kT)$, where k is the Boltzmann constant and T is the temperature. As can be seen, the decrease in the $V_{[Ni^{2+}]}$ displays a diminution of logσ, which is probably connected with a decrease of the density of interstitial Pb^{+2} ions. For the PbSNi06 sample in the middle, the (dark conductivity) DC line shape has a wide band, probably as a consequence of an intracrystalline disorder. The DC is observed to decrease when the doping is increased with a decrease in temperature in these films. It can be seen that the data cannot be filled by a single straight line in the entire temperature range for the films with different doping levels. A decrease in GS with an increase in doping indicates that the observed decrease of logσ in nanoparticle films is a result of change in the packing density of particles. The DC data do not show Arrhenius behaviour, except for a limited temperature range above 200 K, as indicated by a straight line. Below this temperature, a gradual decrease in activation energy with a decrease in temperature is observed in films with different doped levels. These results are similar

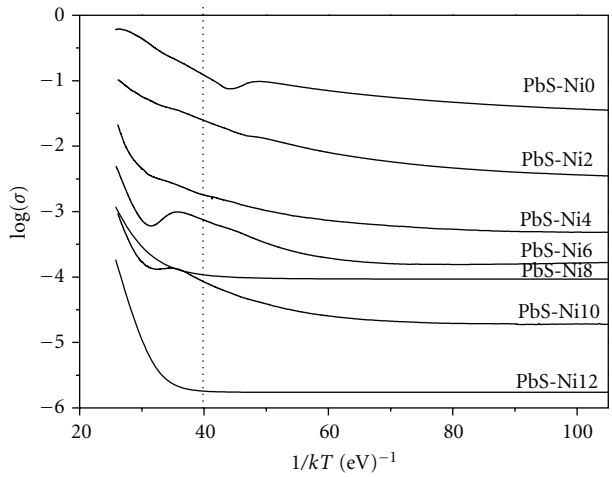

Figure 11: $\log\sigma$ as function of T^{-1}, in the temperature range for doped-PbS films.

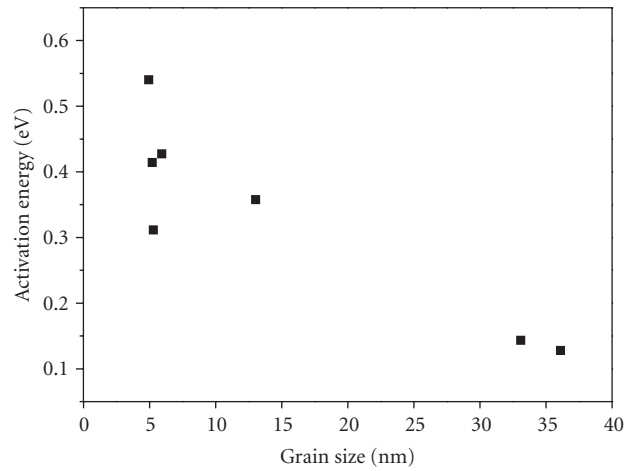

Figure 13: Activation energies versus grain size (GS) for undoped and doped-PbS.

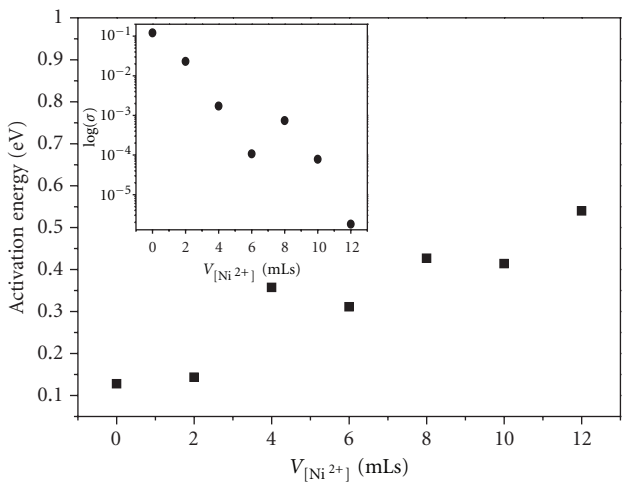

Figure 12: Activation energies (E_a) versus $V_{[Ni^{2+}]}$ for undoped- and doped-PbS films. The inset exhibits E_g versus $V_{[Ni^{2+}]}$.

to those observed in nanocrystalline $Pb_{1-x}Fe_xS$ [31]. The transport mechanism has been explained through a Pb excess or thermal intrinsic disorder of lattice atoms and irreversible changes in the crystalline structure. This assumption is supported by the fact that for cubic PbSNi0, stabilizing effects are provided by the substrate-deposit lattice match and presence of staking disorder. Since we employed amorphous glass substrates, the lattice of cubic samples can be affected by large density of staking faults.

Figure 12 shows the plot of activation energies (E_a) versus $V_{[Ni^{2+}]}$ for undoped and doped PbS films. The fact that $\log\sigma$ versus T^{-1} data do not show Arrhenius behaviour indicates that the carriers do no become activated to a mobility edge above which the extended state take places. The gradual decrease in E_a with a decrease in temperature suggests that the conduction is by hopping of carriers among localized states. The inset of Figure 12 displays $\log\sigma$ versus $V_{[Ni^{2+}]}$. The observed difference in the DC of the doped films can be ascribed to (i) the creation of a new defect, and (ii) the increase in the high barrier between doped-PbS nanocrystals. It must be noted that the increase of E_a and diminution of DC in doped layers can be related to a stronger compensation of the Ni^{2+} donor and, in this regard, we deem that the high resistance of the nanocrystalline films is due to small crystallite sizes. Change in crystallite size will mainly affect the mobility of the carriers and therefore change the resistance. The thermal E_a for films was calculated from the slope of $\log\sigma$ curve versus temperature. This energy was estimated to be 0.15 to 0.5 eV. For PbS films, two sensitizing canters were established with E_a values of approximately 0.13 and 0.22 eV [32]. Figure 13 shows the plot of activation energies E_a versus grain size (GS) for undoped and doped films. Recently, percolation methods were developed based on potential fluctuation due to intercrystalline barriers. Neither of these models can explain all the experimental features of PbS films, but showed that the structural properties play a decisive role in conductivity of the chemically deposited PbS films. As a result of earlier investigations, it was found that there is an optimum grain size in PbS doped with $Ni^{2+}$for which the conductivity signal reaches a maximum. While the single semiconductors quantum dot is relatively well understand, the understanding of the physical properties of dense ensembles of quantum dots is still at a rudimentary level. In particular, while considerable advances in the evaluation of the optical properties and in the interdot conduction mechanics in such ensembles have been reported, correlation was made between their macroscopic, disorder-semiconductor like transport and phototransport properties, the confinement induced level shifts in the corresponding individual nanocrystallites. However we have previously reported that crystallite-size dependence of the transport and phototransport properties in solid-state ensembles of semiconductor quantum dots by finding a Meyer-Neldel-like behaviour for the former and by comparing the experimental results with computer simulations for the latter showed that the aforementioned evidence were associated with the

quantum confined induced variation of the bandgap in the individual dots [22].

CBD of the films is known to occur in two steps, first of which is nucleation and the second is growth [33]. As soon as we dip the slide in the chemical bath, centers of nucleation are formed on the surface of the slide, and with time the cluster growth on these centers of nucleation takes place at the same time new centers of nucleation are created on surface of the slide. For doped films with high concentration of Ni^{2+}, growth of the centers occurs at a critical point where precipitation takes place. The precipitation of critical size clusters leads to the formation of very small particles. Some of these precipitates, in turns, are deposited on the growing clusters while others form new nucleation centers, Initially, due to high concentration of Cd^{2+}, Ni^{2+}, and S^{2-}, the rate of formation of nucleation centers, cluster growth, and cluster precipitation will be high and will decrease with time due to decreasing ionic concentrations of solution. An initial snapshot of the distribution of cluster size, will show them to be a very small mean size, however, with increasing concentration we observe a decrease in the average size of clusters. In addition, the size dispersion and the density of the clusters will also increase. The better crystallinity of the PbSNi12 film can be related to density of critical size clusters, since a higher density of critical sized cluster will make the film of better crystalline quality. Let R_c be the radius of cluster (critical size) at which its precipitation occurs, and let R be the radius of any other cluster, such that $|R - R_c| < \varepsilon$, where ε is very small. The density $\rho(R)$ of the clusters having size R is zero, the concentration of Pb^{2+}, Ni^{2+}, and S^{2-} in the solution will decrease, making the rate of cluster growth infinitesimally slow. Thus, with increasing concentration the density of critical sized cluster, $\rho(R)$, will at first increase and after attaining a maximum value will then slowly approach to zero. Hence, the better crystallinity of doped samples is attributed to higher density of critical size cluster which attain a maximum value will slowly approach to zero.

4. Conclusions

We have reported the growth of doped-PbS with Ni^{2+} ions affording nanocrystalline films by the chemical bath technique. X-ray spectra show $2\theta = [26.00, 30.07, 43.10, 51.00, 53.48]$, which belong to the ZB phase. The grain size lies in the interval of ~3.2–5 nm. The ID for low $V_{[Ni^{2+}]}$ concentrations into the PbS lattice increases and reaches maxima values for intermediates $V_{[Ni^{2+}]}$. TEM image for nanoparticle films of the undoped- and doped-PbS were obtained, the micrographswith an electron beam direction close (111) zone axis in strongly under focused condition with nanoparticle doped in the range 3.5–5 nm. The average grain size in the films decreases while doping increase. Samples are found to be crystalline by TEM and very similar to size calculated from XRD peak width. Optical absorption spectra are quantified for the PbSCd10 film in which the redshift of bandgap is associated with the decrease of the average TG. The E_g of films increased from 2.4 to 3.8 eV when doping $V_{[Ni^{2+}]}$ is increased. GS reduces in the interval 2 mLs $\leq V_{[Ni^{2+}]} \leq$ 12 mLs and an E_g increases as function of the GS is displayed. When GS $\cong$ 5 nm, E_g reaches a maximum value; for larger GS, E_g decreases. We deem two effects occur on E_g changes: (i) the variation of ID and (ii) the quantum confinement. The thermal E_a for films was determined from the slope of log σ curve versus temperature. This energy was estimated to be 0.15 to 0.5 eV.

Acknowledgments

The authors thank P. Hugo Hernandez Tejeda, de la VIEP and Lic. R. Villegas Tovar, director de la Bibliotheca Niels Bohr, J. G. Quiroz Oropeza director de la Fac. De Ciencias Químicas of the Benemérita Universidad Autónoma de Puebla for the support given to the publication of this work.

References

[1] A. P. Gaiduk, P. I. Gaiduk, and A. N. Larsen, "Chemical bath deposition of PbS nanocrystals: effect of substrate," *Thin Solid Films*, vol. 516, no. 12, pp. 3791–3795, 2008.

[2] R. K. Joshi, A. Kanjilal, and H. K. Sehgal, "Size dependence of optical properties in solution-grown Pb1-xFexS nanoparticle films," *Nanotechnology*, vol. 14, no. 7, pp. 809–812, 2003.

[3] Y. F. Nicolau, M. Dupuy, and M. Brunel, "ZnS, CdS, and $Zn_{1-x}Cd_xS$ thin films deposited by the successive ionic layer adsorption and reaction process," *Journal of the Electrochemical Society*, vol. 137, no. 9, pp. 2915–2924, 1990.

[4] S. C. Ray, M. K. Karanjai, and D. DasGupta, "Deposition and characterization of $Zn_xCd_{1-x}S$ thin films prepared by the dip technique," *Thin Solid Films*, vol. 322, no. 1-2, pp. 117–122, 1998.

[5] L. P. Deshmukh, K. M. Garadkar, and D. S. Sutrave, "Studies on solution grown $Hg_XCd_{1-X}S$ thin films," *Materials Chemistry and Physics*, vol. 55, no. 1, pp. 30–35, 1998.

[6] O. Portillo-Moreno, H. Lima-Lima, V. Ramírez-Falcon et al., "Growth of CdS: Cu nanocrystals by chemical synthesis," *Journal of the Electrochemical Society*, vol. 153, no. 10, pp. G926–G930, 2006.

[7] V. M. García, M. T. S. Nair, and P. K. Nair, "Optical properties of $PbSCu_xS$ and $Bi_2S_3Cu_xS$ thin films with reference to solar control and solar absorber applications," *Solar Energy Materials and Solar Cells*, vol. 23, no. 1, pp. 47–59, 1991.

[8] J. B. Biswal, N. V. Sawant, and S. S. Garje, "Deposition of rod-shaped antimony sulfide thin films from single-source antimony thiosemicarbazone precursors," *Thin Solid Films*, vol. 518, no. 12, pp. 3164–3168, 2010.

[9] K. Rakesh, A. K. Joshi, and H. K. Shegal, "Solution grown PbS nanoparticle films," *Applied Surface Science*, vol. 221, pp. 43–47, 2004.

[10] S. Thangavel, S. Ganesan, S. Chandramohan, P. Sudhagar, Y. S. Kang, and C. H. Hong, "Band gap engineering in PbS nanostructured thin films from near-infrared down to visible range by in situ Cd-doping," *Journal of Alloys and Compounds*, vol. 495, no. 1, pp. 234–237, 2010.

[11] M. Wanili, J. M. Luther, H. Zheng, Y. Wu, and P. Alivisatos, "Photovoltaic Devices Employing Ternary PbS_xSe_{1-x} Nanocrystals," *Nanoletters*, vol. 9, pp. 1699–1703, 2009.

[12] S. Wu, H. Zeng, and Z. A. Schelly, "Preparation of ultrasmall, uncapped PbS quantum dots via electroporation of vesicles," *Langmuir*, vol. 21, no. 2, pp. 686–691, 2005.

[13] J. Ju, D. Cui, T. Zhu et al., "The effect of added oversized elements on the microstructure of binary alloy nanoparticles," *Nanotechnology*, vol. 17, pp. 1699–1703, 2006.

[14] W. U. Huynh, J. J. Dittmer, and A. P. Alivisatos, "Hybrid nanorod-polymer solar cells," *Science*, vol. 295, no. 5564, pp. 2425–2427, 2002.

[15] J. M. Pietryga, R. D. Schaller, D. Werder, M. H. Stewart, V. I. Klimov, and J. A. Hollingsworth, "Pushing the band gap envelope: mid-infrared emitting colloidal PbSe quantum dots," *Journal of the American Chemical Society*, vol. 126, no. 38, pp. 11752–11753, 2004.

[16] A. J. Bethune and N. A. S. Loud, *Standard Aqueous Potential An Temperature Coefficients at 25∘C*, vol. 2, Hampel, Skokie, Ill, USA, 1969.

[17] O. Portillo-Moreno, H. Lima-Lima, R. Lozada-Morales, R. Palomino-Merino, and O. Zelaya-Angel, "Cd(S(1-x) + CO3(x)) thin films by chemical synthesis," *Journal of Materials Science*, vol. 40, no. 17, pp. 4489–4492, 2005.

[18] E. Pentia, L. Pintilie, I. Matei, T. Botila, and E. Ozbay, "Chemically prepared nanocrystalline PbS thin films," *Journal of Optoelectronics and Advanced Materials*, vol. 3, no. 2, pp. 525–530, 2001.

[19] R. Kostic, M. Romcevic, N. Romcevic et al., "Photoluminescence and far-infrared spectroscopy of PbS quantum dots—polyvinyl alcohol nanocomposite," *Optical Materials*, vol. 30, pp. 1177–1182, 2010.

[20] J. U. Lunz, Khun, F. Goschenhofer et al., "Temperature dependence of the energy gap of zinc−blende CdSe and $Cd_{1-x}Zn_xSe$ epitaxial layers ," *Journal of Applied Physics*, vol. 80, pp. 6861–6863, 1996.

[21] B. K. Rai, H. D. Bist, R. S. Katiyar, M. T. S. Nair, P. K. Nair, and A. Mannivannan, "Simultaneous observation of strong and weak quantum confinement effect in chemically deposited CdSe thin films: a spectro-structural study," *Journal of Applied Physics*, vol. 82, no. 3, pp. 1310–1319, 1997.

[22] I. Balberg, E. Savir, Y. Dover, O. P. Moreno, R. Lozada-Morales, and O. Zelaya-Angel, "Meyer-Neldel-like manifestation of the quantum confinement effect in solid ensembles of semiconductor quantum dots," *Physical Review B*, vol. 75, no. 15, Article ID 153301, pp. 153301–15304, 2007.

[23] A. Rivera-Márquez, M. Rubín-Falfán, R. Lozada-Morales et al., "Quantum confinement and crystalline structure of CdSe nanocrystalline films," *Physica Status Solidi A*, vol. 188, no. 3, pp. 1059–1064, 2001.

[24] A. Popa, M. Lisca, V. Stancu, M. Buda, E. Pentia, and T. Botila, "Crystallite size effect in PbS thin films grown on glass substrates by chemical bath deposition," *Journal of Optoelectronics and Advanced Materials*, vol. 8, no. 1, pp. 43–45, 2006.

[25] H. Fan, K. Yang, D. M. Boye et al., "Self-Assembly of Ordered, Robust, Three-Dimensional Gold Nanocrystal/ Silica Arrays," *Science*, vol. 304, no. 5670, pp. 567–571, 2004.

[26] R. Sherwin, R. J. H. Clark, R. Lauck, and M. Cardona, "Effect of isotope substitution and doping on the Raman spectrum of galena (PbS)," *Solid State Communications*, vol. 134, no. 8, pp. 565–570, 2005.

[27] A. Phuruangrat, T. Thongtem, and S. Thongtem, "Characterization and photoluminescence of pbs nanocubes synthesized by a solvothermal method," *Chalcogenide Letters*, vol. 8, no. 5, pp. 297–300, 2011.

[28] G. D. Smith, S. Firth, R. J. H. Clark, and M. Cardona, "First- and second-order Raman spectra of galena (PbS)," *Journal of Applied Physics*, vol. 92, no. 8, p. 4375, 2002.

[29] S. Xiong, B. Xi, D. Xu et al., "L-cysteine-assisted tunable synthesis of PbS of various morphologies," *Journal of Physical Chemistry C*, vol. 111, no. 45, pp. 16761–16767, 2007.

[30] K. K. Nanda, S. N. Sahu, R. K. Soni, and S. Tripathy, "Raman spectroscopy of PbS nanocrystalline semiconductors," *Physical Review B*, vol. 58, no. 23, pp. 15405–15407, 1998.

[31] R. K. Joshi and H. K. Sehgal, "Structure, conductivity and Hall effect study of solution grown $Pb_{1-x}Fe_xS$ nanoparticle films," *Nanotechnology*, vol. 14, no. 6, pp. 592–596, 2003.

[32] K. K. Nanda, S. N. Sahu, R. K. Soni, and S. Tripathy, "Raman spectroscopy of PbS nanocrystalline semiconductors," *Physical Review B*, vol. 58, no. 23, pp. 15405–15407, 1998.

[33] R. Garuthara and G. Levine, "Photoluminescence of chemically deposited CdSe nanocrystallites: effects of crystallite polydispersity," *Journal of Applied Physics*, vol. 80, no. 1, pp. 401–405, 1996.